Tumor-Penetrating Peptide Enhances Antitumor Effects of IL-24 Against Prostate Cancer

Jie Yang[*, 1], Hong Yin[*, †, 1], Jie Yang[*, †], Yanhong Wei[*, ‡], Lin Fang[*], Dafei Chai[*], Qing Zhang[*] and Junnian Zheng[*, †, §, ¶]

[*]Cancer Institute, Xuzhou Medical University, Xuzhou 221002, China; [†]Center of Radiotherapy of The Second Affiliated Hospital of Xuzhou Medical University, Xuzhou 221002, China; [‡]Center of Cancer of The Central Hospital of Yongzhou, Yongzhou 425000, China; [§]Center of Clinical Oncology, Affiliated Hospital of Xuzhou Medical University, Xuzhou, Jiangsu 221002, China; [¶]Jiangsu Center for the Collaboration and Innovation of Cancer Biotherapy, Cancer Institute, Xuzhou Medical University, Xuzhou 221002, China

Abstract

The interleukin-24 (IL-24), a member of the IL-10–related cytokine gene family, is well known for its tumor suppressor activity in a broad spectrum of human tumors without damaging normal cells. However, poor tumor penetration remains a key problem for the efficacy of IL-24 as a treatment. iRGD is a novel tumor-specific peptide with unique tumor-penetrating and cell-internalizing properties. To enhance the tumor-penetrating and antitumor effects of IL-24, we engineered a recombinant protein consisting of the IL-24 fused to iRGD, which was named IL-24-iRGD. The aim of the present study was to investigate the antitumor effects of IL-24-iRGD in prostate cancer cells *in vitro* and *in vivo*. It was observed that IL-24-iRGD induced cell apoptosis, suppressed cell growth of PC-3 *in vitro*, and promoted protein penetration into tumors *in vivo*, whereas it had no effect on normal cell line RWPE-1. Then, PC-3 cells were subcutaneously injected into nude mice, and these tumor-bearing mice were administered with IL-24, IL-24-iRGD, or PBS *via* the tail vein. The IL-24– and IL-24-iRGD–treated groups exhibited tumor growth inhibition rates of 38.6% and 65.6%, respectively, when compared with the PBS-treated group. Besides, cell apoptosis was examined by TdT-mediated dUTP nick end labeling, and the expression of cleaved caspase-3 was analyzed by immunohistochemical staining. The results demonstrated that IL-24-iRGD induced apoptosis and inhibited the growth of PC-3 cells to a significantly greater extent when compared with IL-24 treatment alone. It may provide an improved strategy for antitumor therapy and the clinical treatment of prostate cancer.

Translational Oncology (2019) **12**, 453–461

Introduction

Prostate cancer (PCa) is the most frequently diagnosed cancer in 105 countries [1] and the second leading cause of cancer-associated mortality in men in America [2] despite improvements in chemo-, radio-, and hormonal therapies [3]. Although PCa may be a slowly progressing disease that allows enough time for early detection, unfortunately, many men who are diagnosed with localized PCa have disease recurrence despite therapy [4]. For that reason, it is imperative to find ways of treating PCa [3].

The interleukin-24 (IL-24) is a member of the IL-10–related cytokine gene family [5] having potent antitumor activity in almost all types of cancers [6]. It has shown significant clinical benefits in patients and is well known for its tumor suppressive activity without damaging normal cells [7,8]. Previous studies have confirmed that IL-24 inhibits

the migration and invasion of PCa cells, selectively inhibits cancer cell growth, and induces apoptosis [9,10]. However, the growth inhibitory effects were mediated by the intracellular and not by extracellular IL-24 protein [10]. Moreover, it was acknowledged that the crossing of the vascular wall and the penetration into the tumor parenchyma against the elevated interstitial pressure in tumors remain major problems to the therapeutic efficacy of most clinical drugs [11,12]. Therefore, the effective delivery of IL-24 to PCa cells and increasing accumulation within the tumor are urgent requirements.

iRGD (CRGDK/RGPDC), developed on the basis of RGD peptides, is a novel tumor-specific peptide with unique tumor-penetrating and cell-internalizing properties [11]. It binds to integrins αvβ3 and αvβ5 and possesses the activity of binding to neuropilin-1 (NRP-1)–dependent cells [13]. Following the initial binding to αv integrins, iRGD is cleaved by proteases to expose the NRP-1 binding site, CRGDK/R, which effectively induces the process of tumor penetration [11]. Due to this novel delivery system and low toxicity in normal cells, iRGD has become a particular focus of location for tumor imaging, diagnosis, and preclinical research [11–14]. Coupled with iRGD, drugs, nanoparticles, and proteins can be effectively delivered to the tumor site, which reduces side effects [14].

In the present study, we prepared recombinant protein in which iRGD was fused with the C-terminal domain of IL-24, termed IL-24-iRGD, and then investigated the antitumor effects of IL-24-iRGD in PCa cells *in vitro* and *in vivo*.

Materials and Methods

Mice and Cell Lines
Male BALB/c nude mice (age, 5-6 weeks) were purchased from the Animal Center of Xuzhou Medical University (Xuzhou, China) and housed in the specific pathogen-free animal facility of the Experimental Animal Center, Xuzhou Medical University. Mice were housed in a temperature (22°C ± 1°C)- and humidity (55% ± 5%)-controlled room with 12-hour light/dark cycles and allowed free access to sterile water and food. All cages housed up to six mice and contained wood shavings and an independent air supply system. All animal procedures performed complied with the National Institutes of Health Guide for the Care and Use of Laboratory Animals.

The human prostate cancer cell line PC-3 and normal human prostate cell line RWPE-1 were obtained from the cell bank of Chinese Academy of Science and available in the authors' laboratory. PC-3 cells were maintained in growth medium containing F-12K medium supplemented with 10% heat-inactivated fetal bovine serum and 100 U/ml penicillin/streptomycin at 37°C under a humidified atmosphere of 95% air–5% CO_2. RWPE-1 cells were maintained in growth medium containing Keratinocyte Serum Free Medium with bovine pituitary extract (0.05 mg/ml) and human recombinant epidermal growth factor (5 ng/ml) in the same culture conditions as PC-3. All reagents were supplied by Gibco.

Construction of IL-24-iRGD Plasmids
The gene sequence of iRGD encoding CRGDKGPDC was fused with Cterminus of IL-24, and the IL-24-iRGD gene sequence was amplified by nested polymerase chain reaction using four oligonucleotide primers from the ZD55-IL-24 plasmid [15]. The sequences were as follows: S1, forward, 5′-CATG **CCATGG** GC *CAT CAT CAT CAT CAT CAT CAT CAT CAT CAC* GCC CAG GGC CAA GAA TTC CAC TTT GG-3′ [bold letters (CCATGG) indicate the

enzyme site of *NcoI* and italic letters represent the histidine (His)-tag]; S2, first reverse primer, 5′-GAA ATT CTA CAA GCT CGG TGG TGG TGG TAG CGG CGG CGG CGG CAG TGG-3′; S3, second reverse primer, 5′-GGC GGC GGC GGC AGT GGT GGC GGT GGC TCT TGC CGC GGC GAC-3′; S4, third reverse primer, 5′-CGC **GGATCC** TTA TTA *GCA GTC GGG GCC CTT GTC GCC GCG GCA* AGA GCC-3′ [italic letters represent the iRGD sequence, and the bold letters (GGATCC) indicate the enzyme site of *BamHI*]. The thermal cycling protocol was as follows: 30 cycles of denaturation at 98°C for 15 seconds, annealing at 55°C for 5 seconds, and polymerization at 72°C for 1 minute, followed by a final polymerization step at 72°C for 10 minutes. The polymerase chain reaction product was digested with *NcoI* and *BamHI* (Thermo Fisher Scientific, Inc.), purified, and cloned into the pET19b vector (maintained in our lab), which had been predigested with *NcoI* and *BamHI*. The generated plasmid was named pET19b-IL-24-iRGD (Figure 1*A*). All construct sequences were confirmed by DNA sequencing (Beijing Genomics Institute/BGI, Shanghai, China).

Expression and Purification of IL-24-iRGD
The pET19b-IL-24-iRGD plasmid was transformed into the BL21 strain of *Escherichia coli (E. coli)*. The bacteria were cultured in LB broth medium (Invitrogen; Thermo Fisher Scientific, Inc.) containing 50 μg/ml ampicillin (Sigma-Aldrich; Merck KGaA, Darmstadt, Germany) at 37°C and efficiently expressed IL-24-iRGD with the isopropyl-β-D-thiogalactoside (IPTG) inducer at a concentration of 1 mmol/l. Following a 10-hour induction period, the bacteria were harvested, resuspended in phosphate-buffered sodium (pH 6.8), and lysed by ultrasonication in ice water at 4°C for 10 minutes. Centrifugation was performed at 16,000×*g* for 20 minutes at 4°C. Urea (8 mol/l) was used to denature the undissolved proteins. The proteins were then purified by Co-NTA His Bind resin chromatography (TALON Metal Affinity Resin; cat. no. 635502; Takara Biotechnology, Co., Ltd., Dalian, China) and eluted with 250 mmol/l imidazole. Renaturation of IL-24-iRGD protein was performed by dialyzing against a low concentration of urea solution (4-0 mol/l). Finally, the purified proteins were dialyzed against water and stored at –80°C following lyophilization. Samples were analyzed by 15% SDS-PAGE analysis (Figure 1*B*).

Western Blot Analysis to Determine the Specificity of Anti–IL-24 Antibodies
Western blotting was used to analyze the specificity of anti–IL-24 antibodies (Figure 1*C*). IL-24-iRGD and IL-24 (PeproTech, cat. no. 96-200-35, USA) were electrophoresed on a 15% SDS-PAGE gel and then transferred to a nitrocellulose membrane (Merck KGaA). The membrane was blocked with 5% bovine serum albumin for 1 hour at room temperature (RT), washed with PBS + Tween 20 (PBST), and probed with a rabbit anti-human IL-24 antibody (dilution, 1:500; cat. no. ab115207; Abcam, Cambridge, MA) for 1 hour at 37°C. This was followed by incubation with a horseradish peroxidase–conjugated goat anti-rabbit IgG secondary antibody (dilution, 1:500; cat. no. VA001; Vicmed Biotech Co., Ltd., Xuzhou, China) for 1 hour at RT. The reaction was completed with 0.05% 3,3′-diaminobenzidine and 0.012% H_2O_2 for 15 minutes at 37°C (Figure 1*C*).

Flow Cytometry
A total of 1×10^6 PC-3 cells were digested with accutase-enzyme cell detachment medium (cat. no. 85-00-4555-56; eBioscience) for

5 minutes at 37°C and washed with PBS twice. And then, cells were incubated with 5 µl fluorescent-labeled antibodies diluted in 100 µl PBS for 30 minutes at RT. The cells were then washed, resuspended, and analyzed using flow cytometer (FACSCanto II; BD Biosciences, Franklin Lakes, NJ). The Annexin V–fluorescein isothiocyanate (FITC)–conjugated mouse anti-human integrin αvβ3 antibody (cat. no. MAB1976F) and integrin αvβ5 antibody (cat. no. MAB1961F) were purchased from Merck KGaA. The matched isotype control antibody, FITC-conjugated mouse IgG1κ, was purchased from eBioscience, Inc. (cat. no. 11-4714-42; San Diego, CA). The phycoerythrin-conjugated mouse anti-human NRP-1 antibody was purchased from Miltenyi Biotec, Inc. (cat. no. 130-098-876; Cambridge, MA). The flow cytometry results were analyzed using flowjo software 7.6.1 (Figure 2A).

Cell Apoptosis Assessment by Flow Cytometry

Annexin V-FITC/propidium iodide (PI) staining was used for cell apoptosis assay. Briefly, PC-3 and RWPE-1 cells (2×10^5/well) were cultured in 6-well plates at 37°C, 5% CO_2, and treated with 60 µg/ml of IL-24-iRGD or IL-24 for 48 hours and then washed twice with PBS. After that, 500 µl Binding Buffer, 5 µl Annexin V-FITC, and 5 µl PI were added to the cells in turn and incubated for 15 minutes at RT. The flow cytometry results were analyzed using flowjo software 7.6.1 (Figure 2, B-E).

Cell counting kit-8 (CCK-8) Method for Cytopathic Assay

In order to assess its cytopathic effect on inhibiting tumor cell growth of IL-24-iRGD *in vitro*, CCK-8 (Tiagen, Beijing, China) was used as instructions. PC-3 and RWPE-1 cells (4×10^3/well) were plated in 96-well plates and treated with 20-100 µg/ml of IL-24-iRGD or IL-24 at 37°C the next day. After incubation for 24, 48, 72, and 96 hours, CCK-8 (10 µl) was added to each well, and the cells

were incubated for 4 hours. Finally, absorbance from the plates was read on an ELX-800 spectrometer (Bio-Tek Instruments Inc., USA) at 450 nm (Figure 3). We set three replicate wells per assay, and each experiment was repeated three times. The maximum value in PBS group was the basis used to calculate cell viability (%).

Tumor Model

PC-3 cells (2×10^6 cells diluted in 100 µl PBS) were subcutaneously injected into the right flank of 30 mice. Tumor-bearing nude mice were randomly divided into PBS, IL-24, or IL-24-iRGD groups at ~4 weeks following injection of PC-3 cells. Assignment of mice into each group was based on tumor size to ensure that there were no statistically significant differences in tumor volume between the groups at the time treatment commenced.

Evaluation of Tumor Tissue Penetration

Four PC-3–bearing mice in each group received an intravenous injection into caudal vein of 10 µg/g IL-24, 10 µg/g IL-24-iRGD, or equal volume of PBS, respectively. At 3 and 7 hours following treatment, the tumors were excised, paraffin embedded, and divided into 4-µm sections (undertaken by pathology department of the affiliated hospital of Xuzhou Medical University, Jiangsu, China). The degree of protein penetration in tumors was analyzed by immunofluorescence. Briefly, tissue sections were stained with a primary rabbit anti-human IL-24 antibody (dilution, 1:100; cat. no. ab115207, Abcam) overnight at 4°C prior to staining with a DyLight 549-conjugated goat anti-rabbit IgG (H + L) secondary antibody (dilution, 1:100; cat no. E032320, Earthox Life Sciences, Millbrae, CA) at 37°C for 1 hour. The sections were then stained with 4′,6-diamidino-2-phenylindole at 37°C for 15 minutes. Tissue sections were analyzed and photographed using a fluorescence microscope (DS-Ri1 Digital Camera; Nikon Corporation, Tokyo, Japan) (Figure 4).
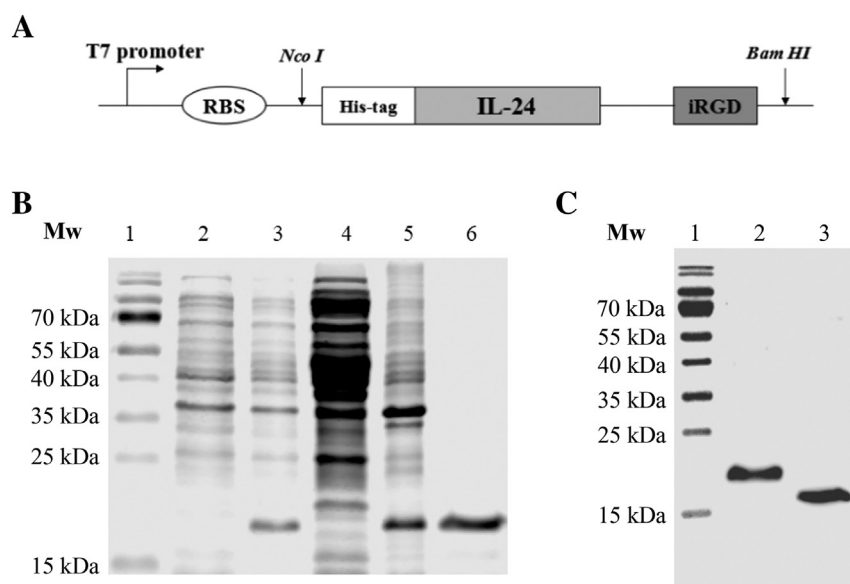

Figure 1. Preparation of IL-24-iRGD-expressing plasmid vector. (A) A schematic of the pET19b-IL-24-iRGD expression vector. A His-tag was attached to the N-terminus of the IL-24 protein, while the iRGD peptide was attached to the C-terminus of the IL-24 protein by linker peptides. (B) 15% SDS-PAGE analysis of the expression and purification of IL-24-iRGD. Lane 1, molecular weight marker; lane 2, total cell protein from BL21 *E. coli* prior to IPTG induction; lane 3, total cell protein from BL21 *E. coli* induced by IPTG; lane 4, protein supernatant following lysis by ultrasonication; lane 5, protein precipitate following lysis; lanes 6, protein sample following purification by affinity chromatography. (C) Western blot analysis of IL-24 and IL-24-iRGD. Lane 1, molecular weight marker; lane 2, IL-24-iRGD; lane 3, IL-24. IL-24, interleukin-24; His, histidine; *E. coli, Escherichia coli;* IPTG, isopropy-β-D-thiogalactoside; Mw, molecular weight.

Treatment In Vivo

The other 18 mice were injected with 10 µg/g IL-24 or IL-24-iRGD, or equal volume of PBS in the tail vein every 3 days, and meanwhile, the tumor volume (Figure 5) and the weight of nude mice were determined. The volume of the tumors was calculated from two diameter measurements using a digital Vernier caliper and the following formula: tumor volume = (length × width^2) / 2. Following five rounds of treatment, all of the mice were sacrificed by neck death for body and tumor weight analysis. The tumor tissues were saturated in 10% formalin solution for 48 hours at RT.

TdT-Mediated dUTP Nick End Labeling (TUNEL) Assay

Tumor tissue sections from mice in each treatment group were formalin fixed, paraffin embedded, and divided into 4-µm sections using the aforementioned procedures. The number of apoptotic cells was detected using an *In Situ* Cell Death Detection kit (Roche)

according to the manufacturer's instructions. The number of TUNEL-positive cells was counted in five fields of view selected at random for each tumor tissue sample ($n = 6$; magnification, ×400), and the apoptotic index in each field was calculated as the percentage of TUNEL-positive cells relative to 100 randomly selected cells. It was undertaken by fluorescent inverted microscope (IX83, Olympus). The integrated optical density (IOD) index for each selected area was analyzed using Image-Pro Plus 6.0 software (Figure 6, A and B).

Expression of Cleaved Caspase-3 in Tumor Tissues

The expression of cleaved caspase-3 was analyzed by immunohistochemical analysis, and the experiments were performed using a streptavidin-peroxidase kit according to the manufacturer's instructions (cat. no. SP9000; ZSGB-BIO, Beijing, China). Briefly, tumor tissues that had been formalin fixed were paraffin embedded and divided into 4-µm sections. The tissue sections were then incubated
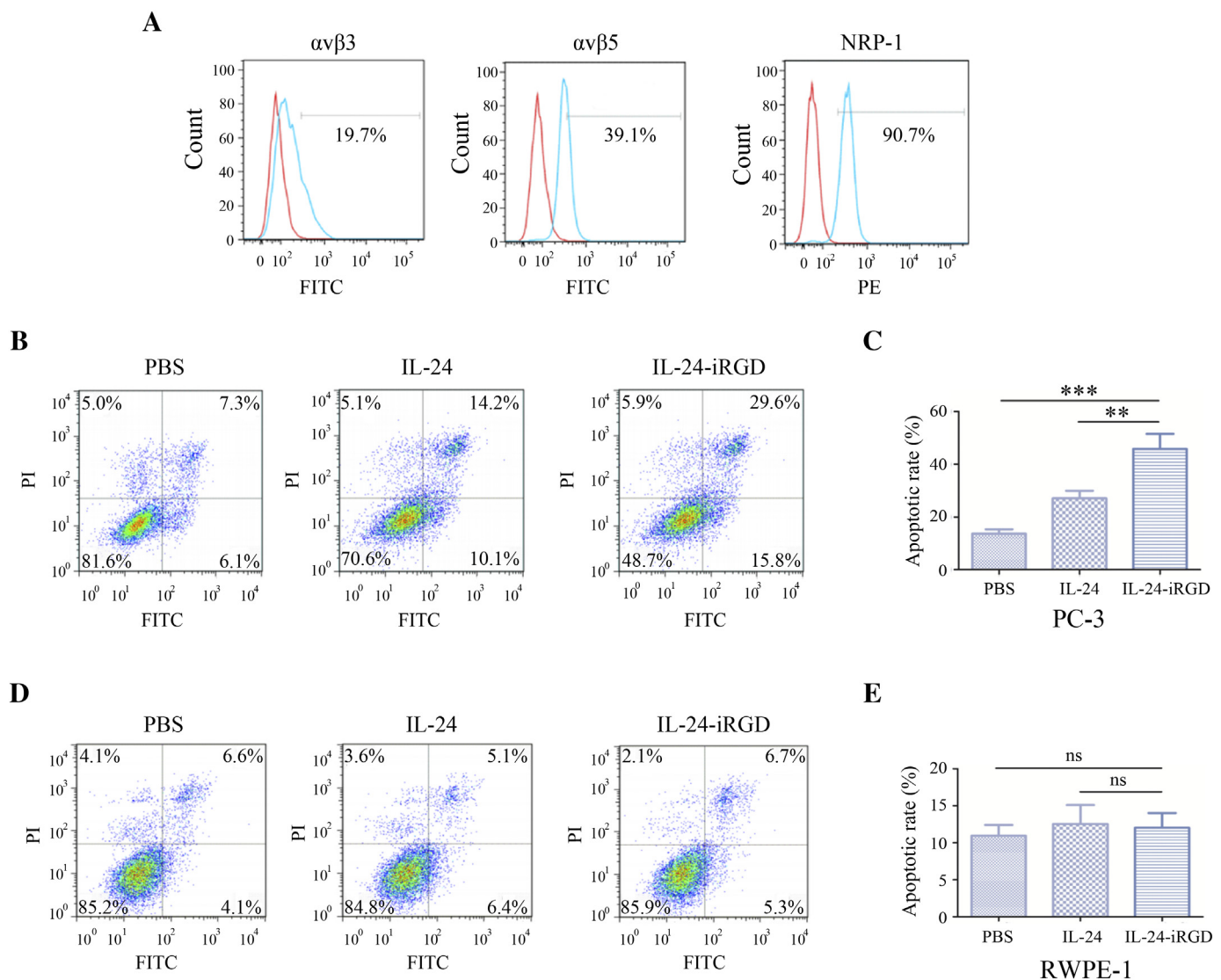

Figure 2. Flow cytometry analysis. (A) Expression analysis of integrin αvβ3 and αvβ5, and NRP-1 in PC-3 cells by flow cytometry. Red line represented the isotype, and the blue line represented the sample. The flow cytometry results were analyzed using flowjo software 7.6.1. PC-3 (B) and RWPE-1 (D) cells (2×10^5/well) were cultured in 6-well plates and treated with 60 µg/ml of IL-24-iRGD or IL-24 for 48 hours. And then Annexin V-FITC/PI staining was used for cell apoptosis assay, and FITC-positive parts represent cell apoptosis, including lower right corners and top right corners. Quantitative representation of the proportion of cell apoptosis analyzed in PC-3 (C) and RWPE-1 (E). Data are expressed as the mean ± SD. $P < .05$, $P < .01$, and $P < .001$, as indicated. ns, not significant.
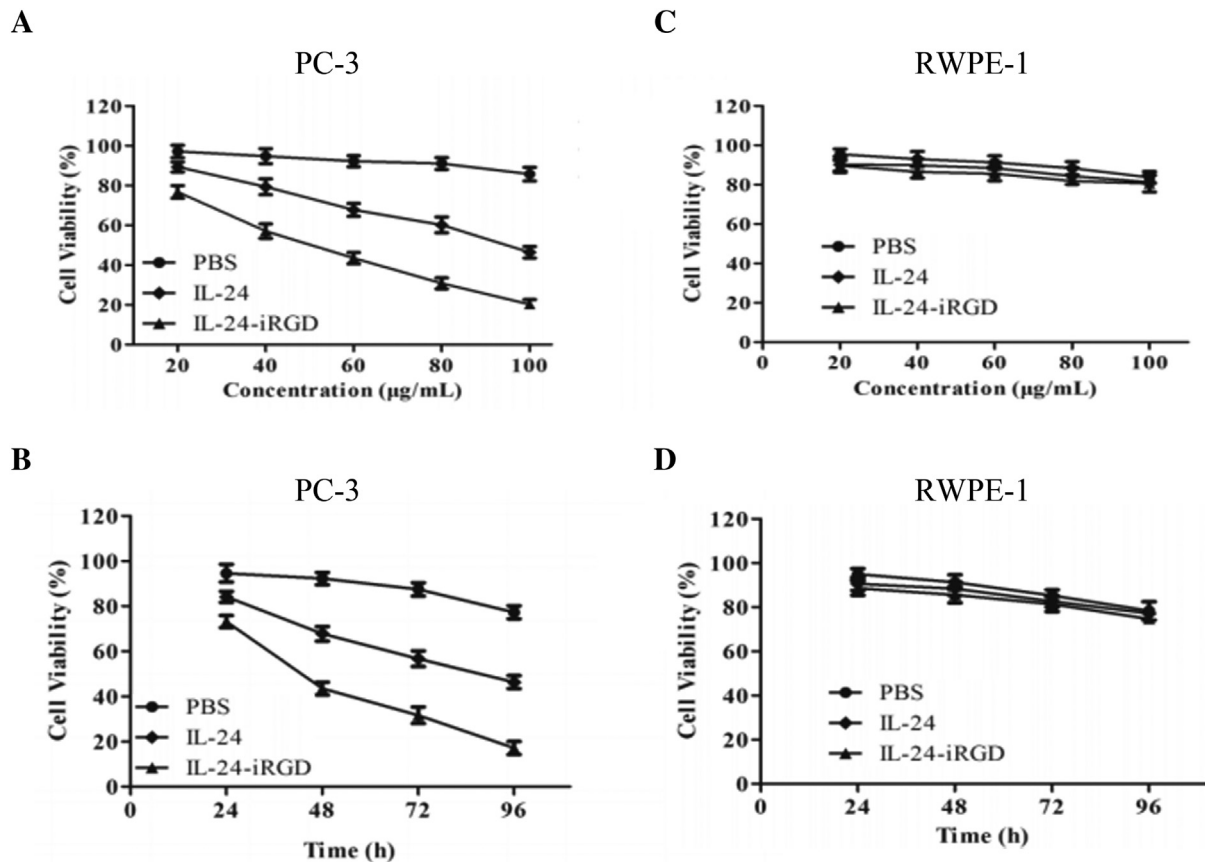
Figure 3. Inhibition and cytopathic effect of IL-24-iRGD on cell growth. PC-3 (A) and RWPE-1 (C) cells were treated with the dose of 20-100 μg/ml of IL-24-iRGD or IL-24 for 48 hours. PC-3 (B) and RWPE-1 (D) cells were treated with the time of 24, 48, 72, and 96 hours, along with the dose of 60 μg/ml of IL-24-iRGD or IL-24. On days 1, 2, 3 and 4 postadministration, cells were subjected to the CCK-8 assay. The maximum value in PBS group was the basis used to calculate cell viability (%). Data are presented as the mean $\pm$ SD from three independent experiments ($n = 3$).

with a rabbit anti-human cleaved caspase-3 antibody (dilution with PBS, 1:100; cat. no. ab13847, Abcam) overnight at 4°C. Following incubation with solutions B and C at 37°C for 30 minutes, respectively, the sections were stained with 50 μl diaminobenzidine for 30 seconds and hematoxylin for 4 minutes at RT. All sections were observed and photographed with a fluorescence microscope (Figure 6C). To determine the IOD index of cleaved caspase-3, five representative fields of view that were positive for cleaved caspase-3 staining were examined for each tumor section ($n = 6$, magnification, ×400). The IOD index for each selected area was analyzed using Image-Pro Plus 6.0 software (Media Cybernetics, Inc., Rockville, MD) (Figure 6D).

Cytopathic Effect Assessment

Hematoxylin and eosin (H&E) staining was used to assess the cytopathic effect of IL-24-iRGD. Briefly, tissues of internal organs were fixed with 4% paraformaldehyde, embedded in paraffin, and cut in 4-μm sections. The slices were deparaffinized with alcohol, washed with distilled water, stained with hematoxylin for 5 minutes, washed with distilled water, restained with eosin for 2 minutes, and then decolorized with distilled water. After dehydration, the slices were made transparent with two treatments of xylene for 1 minute each. Finally, the slices were mounted with neutral gum to be observed under the microscope (Figure 7B).

Statistical Analysis

Quantitative data are presented as the mean ± standard deviation (SD). An independent-samples t test was used to compare two groups. $P < .05$ was considered to indicate a statistically significant difference.

Results

Construction, Expression, and Purification of IL-24-iRGD

The pET19b-IL-24-iRGD vector was generated to express IL-24-iRGD (Figure 1A). IL-24-iRGD (molecular weight, 21 kDa) was efficiently expressed in recombinant BL21 *E. coli* and purified by affinity resin chromatography to approximate homogeneity on a 15% SDS-PAGE gel (Figure 1B). In addition, IL-24 and IL-24-iRGD were analyzed by Western blot using an anti–IL-24 antibody to verify the correct preparation of the proteins (Figure 1C).

Expression of $\alpha v\beta 3$, $\alpha v\beta 5$, and NRP-1 in PC-3

To verify whether PC-3 was suitable for this experiment, expression of $\alpha v\beta 3$, $\alpha v\beta 5$, and NRP-1 in PC-3 cells was tested by flow cytometry. As shown in Figure 2A, the positive expression rates of $\alpha v\beta 3$, $\alpha v\beta 5$, and NRP-1 were 19.7%, 39.1%, and 90.7%, respectively. These results demonstrated that the PC-3 cell line may be useful for the establishment of a human PCa model to study the effects of IL-24-iRGD.
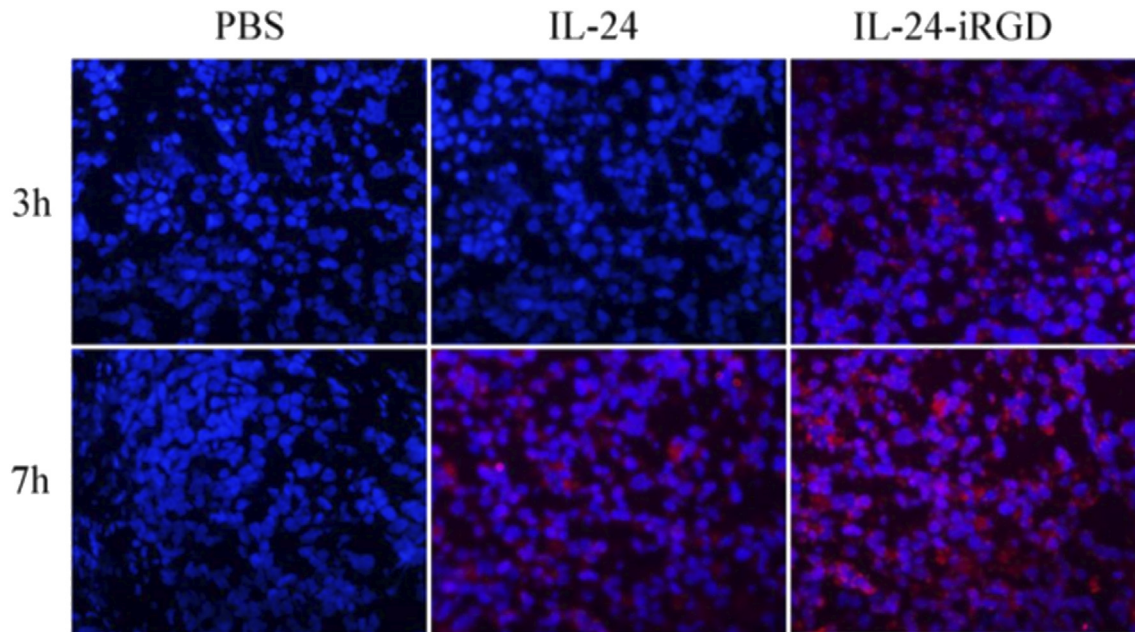
Figure 4. Analysis of the penetration of IL-24 in PC-3 tumor tissues. A total of 10 μg/g of IL-24 or IL-24-iRGD was injected into the tail vein of PC-3–bearing mice. After 3 and 7 hours of treatment, the penetration of IL-24 in PC-3 xenograft tumors was detected by immunofluorescence staining. $n = 4$; magnification, ×400. Red staining indicates IL-24 protein, and blue represents DAPI staining, indicating the nucleus. DAPI, 4′,6-diamidino-2-phenylindole.

Apoptosis by Annexin V-FITC/PI Staining

Besides, Annexin V-FITC/PI staining and flow cytometry were used for cell apoptosis assay *in vitro*. As shown in Figure 2, FITC positivity of PC-3 cells of IL-24-iRGD group was significantly more than that of PBS group ($P < .001$) (Figure 2, *B* and *C*), whereas there were no significant difference in the FITC positivity of RWPE-1 cells of groups (Figure 2, *D* and *E*). These results suggested that IL-24-iRGD could effectively induce tumor cell (PC-3) apoptosis *in vitro* but have no effect on normal cell line RWPE-1.

CCK-8 Assay

Here, CCK-8 assay was used to assess its cytopathic effect on inhibiting tumor cells growth of IL-24-iRGD *in vitro*. We compared the results of the treatments with the time of 24, 48, 72, and 96 hours, and the dose of 20-100 μg/ml of IL-24-iRGD or IL-24. As shown in Figure 3, PC-3 (*A*) and RWPE-1 (*C*) cells were treated with the dose of 20-100 μg/ml of IL-24-iRGD or IL-24 for 48 hours. PC-3 (*B*) and RWPE-1 (*D*) cells were treated with the time of 24, 48, 72, and 96 hours, along with the dose of 60 μg/ml of IL-24-iRGD or IL-24. CCK-8 results demonstrated that both of IL-24-iRGD and IL-24 could inhibit tumor cell (PC-3) growth *in vitro* and result in dose-time dependence (Figure 3, *A* and *B*), while they had no effect on normal cell line RWPE-1 (Figure 3, *C* and *D*). Besides, the treatment of IL-24-iRGD had higher inhibition ability than the other groups. The data showed that IL-24-iRGD effectively inhibited PC-3 cell proliferation *in vitro*.

Tumor Tissue Penetration

In order to confirm the *in vivo* effects of the tumor-penetrating peptide iRGD and examine the expression of IL-24 in tumor tissues, we developed a BALB/c nude mouse model using the human PC-3 cell line. The penetration of IL-24 into tumors was determined by immunofluorescence staining. As shown in Figure 4, IL-24 displayed modest binding to the surface of the tumor tissue following injections at 3 and 7 hours, whereas IL-24-iRGD bound strongly, and even penetrated, several cell layers into the tumor tissue. The results demonstrated that iRGD effectively enhanced the penetration of IL-24 into tumor tissues.

Therapeutic Efficacy of IL-24-iRGD Against PC-3 In Vivo

To examine the therapeutic efficacy of IL-24-iRGD, the PC-3 mouse xenograft tumor model was first established. A schematic of the tumor model and treatment of mice was shown in Figure 5*A*. The rate of tumor growth in the IL-24-iRGD group was reduced when compared with the IL-24 group, and the tumor volume of the IL-24-iRGD group was significantly reduced when compared with the PBS ($P < .001$) and IL-24 groups (P < .001; Figure 5, *B* and *C*). These observations were confirmed by an analysis of the tumor weight in each group ($P < .001$; Figure 5, *D*). The rate of tumor growth inhibition was then analyzed further. Tumor inhibition (%) was calculated by the subtraction and division of average weight of tumors in PBS group and IL-24 or IL-24-iRGD group. At the end of the experiment, tumors from mice in the IL-24 group and the IL-24-iRGD group exhibited growth inhibition rates of 38.6% and 65.6%, respectively (Figure 5, *E*). These results demonstrated that iRGD efficiently enhanced the therapeutic efficacy of IL-24 in human PC-3 cells *in vivo*.

Apoptosis Analysis of Tumor Tissue

Next, to assess and verify the apoptosis of tumor tissue, TUNEL and the expression of cleaved caspase-3 were analyzed by immunohistochemical staining. As shown in Figure 6, *A* and *B*, tumors from mice in the IL-24-iRGD group exhibited significantly stronger TUNEL staining (the brown) when compared with tumors from mice treated with PBS or IL-24, which indicated substantial cell apoptosis in the IL-24-iRGD–treated tumors (P < .001). Similarly,
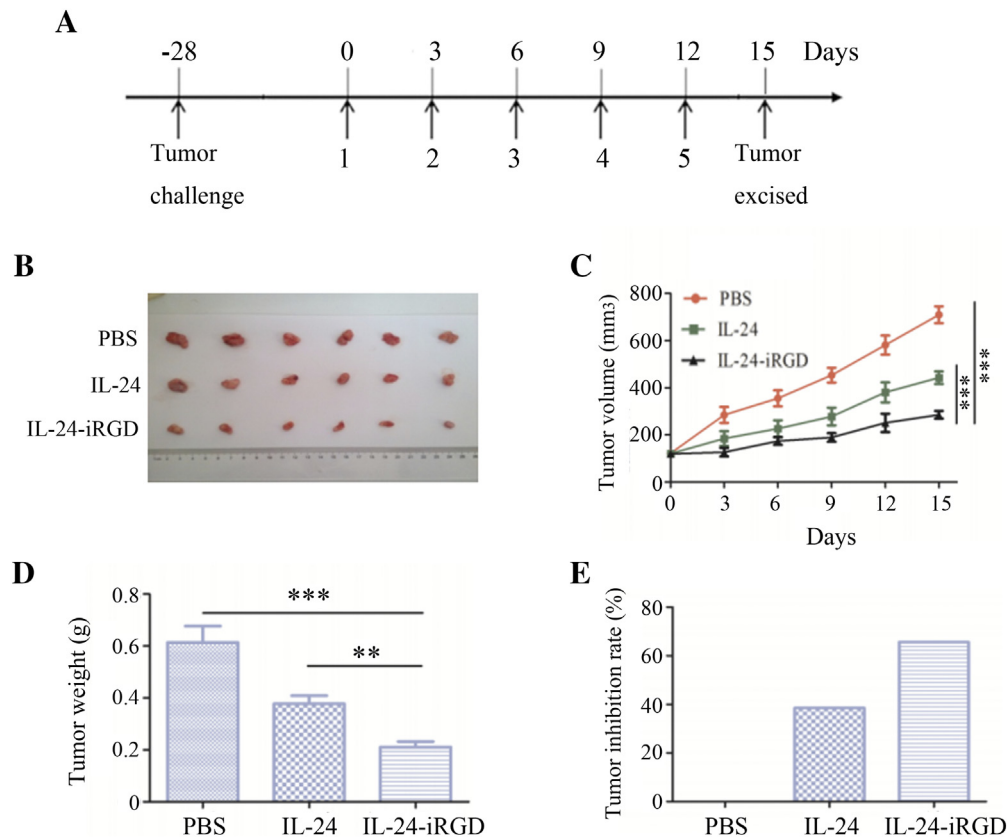
Figure 5. Therapeutic efficacy of IL-24-iRGD *in vivo*. Mice were injected with 10 μg/g IL-24 or IL-24-iRGD, or equal volume of PBS in the tail vein every 3 days. Following five rounds of treatment, all of the mice were sacrificed. (A) Establishment of the PC-3-mouse tumor model and treatment regimen. (B) Solid tumors excised from mice injected with PBS, IL-24, or IL-24-iRGD ($n = 6$). (C) Tumor volume over the course of treatment. Tumor volume was measured once every 3 days until day 15. (D) Comparison of the average tumor weight in each group at the end of treatment. (E) Tumor inhibition rate of IL-24 and IL-24-iRGD. Tumor inhibition (%) = ($W_{PBS} - W_{IL-24-iRGD}$)/W_{PBS}. Data are expressed as the mean ± SD. $P < .05$, $P < .01$, and $P < .001$, as indicated.

the results shown in Figure 6, *C* and *D* revealed a significant increase in cleaved caspase-3 expression in the tumor tissues from mice in the IL-24-iRGD group when compared with the PBS ($P < .001$) and IL-24 groups ($P < .01$).

Mice Body Weight Analysis

To evaluate the influence of IL-24-iRGD to mice, the body weight of mice in each experimental group was assessed. As shown in Figure 7A, there was no significant difference in the PBS, IL-24, or IL-24-iRGD groups.

H&E Analysis

Finally, to assess the cytopathic effect on mice of IL-24-iRGD, the slices of heart, liver, spleen, lung, and kidney of treated mice were analyzed by H&E staining. As shown in Figure 7B, there was no significant difference in the PBS, IL-24, or IL-24-iRGD groups. These data showed that IL-24-iRGD was safe to these organs of the mice.

Discussion

The aim of the present study was to assess the use of iRGD peptide as a tool for improving the delivery and therapeutic efficacy of IL-24 treatment against PCa. The results demonstrated that it enhanced the accumulation and therapeutic efficacy of IL-24 in mouse PC-3

xenograft tumors, which were established using the PC-3 cell line that exhibited high expression levels of αvβ3, αvβ5, and NRP-1. In addition, the results demonstrated that the IL-24-iRGD protein induced apoptosis, accelerated cell death, and inhibited tumor cell growth to a greater extent than IL-24 treatment alone. This was considered to be due to the efficient iRGD-mediated increase in the tumor penetration ability of IL-24 in human prostate tumors.

Previous studies have confirmed that IL-24 is a multifaceted killer of numerous cancer cells that has shown great clinical benefit in patients [8]. However, as we mentioned above, the crossing of the vascular wall and the penetration into the tumor parenchyma against the elevated interstitial pressure in tumors remain major obstacles to the therapeutic efficacy of IL-24 and other drugs [11,12]. The low concentration of anticancer drugs at the tumor site is a substantial barrier for tumor treatment, which limits the anticancer efficacy and suggests that the effective drug concentration at the tumor site is markedly lower compared with the dose of exposure [14]. Thus, research investigating IL-24 as an anticancer treatment has employed adenoviruses as carriers for transfecting cancer cells with the IL-24 gene, and IL-24 is a well-studied cytokine established as a therapeutic in a wide array of cancers upon delivery as a gene therapy [9,10]. This method has demonstrated satisfactory anticancer effects. However, adenoviral delivery of genes against cancer has been faced with many problems, such as their cancer-specific targeting ability and safety
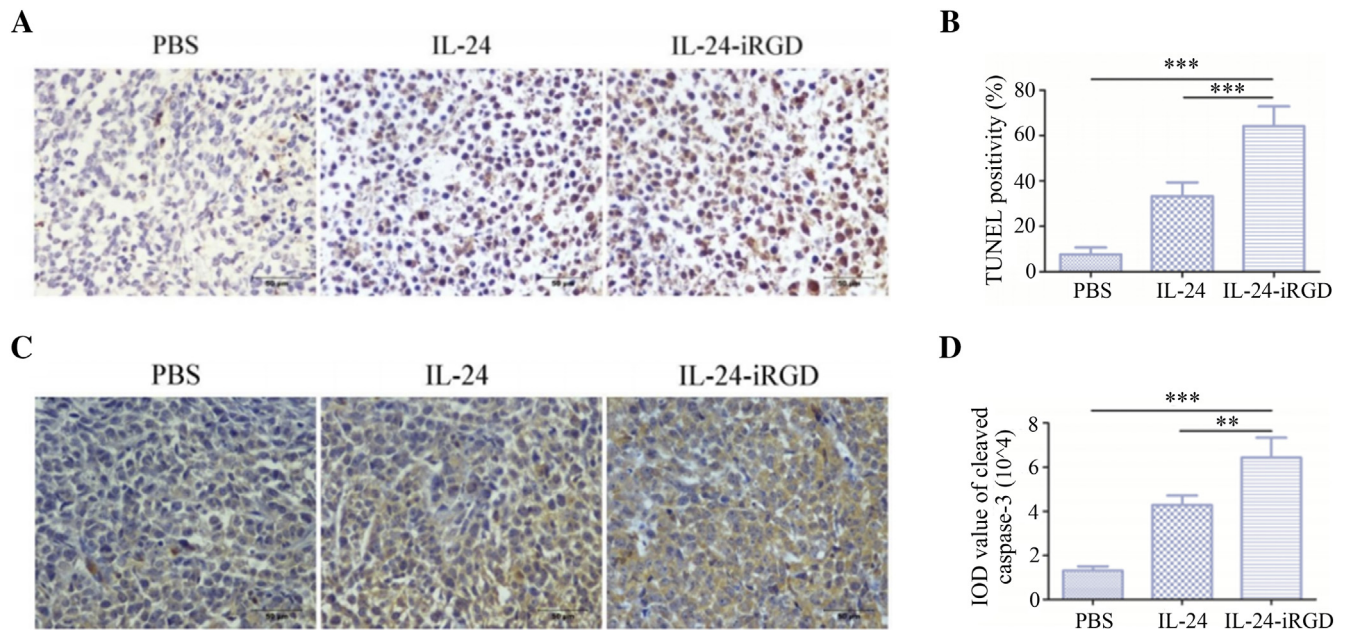
Figure 6. Immunohistochemical analysis of PC-3 xenograft tumor tissues. (A) Representative microscope images of TUNEL-stained tumor tissue sections derived from mice treated with PBS, IL-24, or IL-24-iRGD. TUNEL-positive nuclei are stained brown, and TUNEL-negative nuclei are stained blue ($n = 6$; magnification, ×400). (B) Quantitative analysis of TUNEL staining in each group. The percentage of TUNEL-positive cells was counted from 100 tumor cells selected at random in each tissue section, and five sections were counted per tumor ($n = 6$). (C) Expression of cleaved caspase-3 in PC-3 tumor xenograft tissues following treatment with PBS, IL-24, or IL-24-iRGD. Brown staining indicates positive cleaved caspase-3 expression, and blue staining indicates cell nuclei. Representative images from each group are shown ($n = 6$; magnification, ×400). (D) Quantitative analysis of cleaved caspase-3 staining in each treatment group. A total of five fields of view for each tumor tissue section were selected at random. IOD values of positively stained regions were calculated using Image-Pro Plus software. Data are expressed as the mean ± SD. Scale bar = 50 μm, $n = 6$. $P < .001$, as indicated.

issues [16]. In 2016, Zhang et al. reported the use of a transactivator of the transcription (TAT 47-57) from human immunodeficiency virus type 1 as a carrier to deliver the IL-24 recombinant protein into cells [16]. The TAT peptide has been demonstrated to deliver various biological molecules, including proteins, DNA, and RNA, into almost all tissues and cell types and even penetrates the blood-brain barrier. However, the high efficiency of penetration into virtually all tissues and cells poses a great risk to human health. It may be considered that the indistinguishableness of TAT penetration could cause serious problems of the brain and other healthy organs.

In the present study, we explored the potential anticancer properties of IL-24 delivered as a recombinant protein. The iRGD peptide was used to overcome this tissue penetration problem, enhancing drug effects against tumors and reducing the drug dose in needed and in other healthy organs. It has been demonstrated that the tumor-penetrating ability of iRGD primarily depends on the expression of $\alpha v\beta3/5$ and NRP-1 in cancer cells [11,12]. The expression of integrins is largely restricted to tumors, and NRP-1 is frequently overexpressed in a number of tumors [17]. Previously, the highly invasive human prostate cancer PC-3 was described as a positive expression model of $\alpha v\beta3$, $\alpha v\beta5$, and NRP-1 [17–19], and it was confirmed in this study. Flow cytometry analysis in our study confirmed that $\alpha v\beta3$, $\alpha v\beta5$, and NRP-1, which mediate the tumor-penetration activity of iRGD, were overexpressed in human PC-3 cell line. In contrast, the noninvasive LNCaP prostate cancer cell line was reported to have negative expression of $\alpha v\beta3$ [18,19]. And DU145 cell line was reported to have positive expression of $\alpha v\beta3$ similar to PC-3 but weak positive expression of $\alpha v\beta5$ [18]. Additionally, RWPE-1 cells were reported to

have positive expression of $\alpha v\beta3$, weak positive expression of $\alpha v\beta5$ [18], but negative expression of NRP-1 [20].

The normal RWPE-1 cells unlike PC-3 cells did not show any additional increase in sensitivity in our study, suggesting that normal cells are resistant to IL-24–mediated killing. Our results are in agreement with the report of Saito et al. [10], who showed normal prostate epithelial cells to be resistant to IL-24. These results suggest that IL-24 selectively inhibits prostate cancer cells, sparing normal cells. The results of H&E staining assays also verified it.

In the *in vivo* xenograft tumor model, tail vein administration of IL-24-iRGD in mice bearing PC-3 significantly inhibited tumor growth, and the suppressive effect was much stronger than that in the IL-24– and PBS-treated groups. These facts are in accordance with the results from *in vitro* studies in which IL-24-iRGD was more effective in growth suppression and apoptosis induction. As shown by immunofluorescence staining assay, much more penetration of IL-24 in tumor tissue was observed in the IL-24-iRGD–treated group. Furthermore, the TUNEL staining and the cleaved caspase-3 expression of tumor slices indicated that tumors treated with IL-24-iRGD induced more extensive apoptosis of tumor cells than those in the IL-24– and PBS-treated groups.

Conclusion
IL-24-iRGD enhanced the effect of IL-24 against PC-3 cells by enhancing penetrating of IL-24, inducing apoptosis, and inhibiting tumor cell growth *in vitro* and *in vivo*. The mechanisms underlying the antitumor effects of IL-24-iRGD against PCa were explored in a preliminary study. The results present a novel strategy for improving
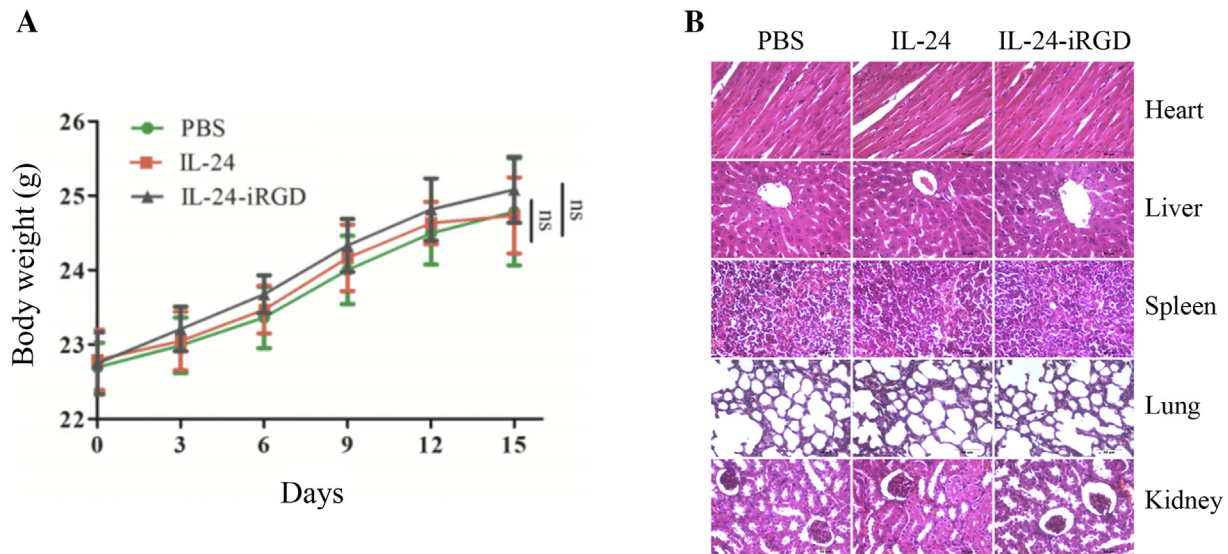
A

B

Figure 7. Toxicity evaluation. (A) Body weights of mice in each group over the course of treatment ($n = 6$). (B) H&E analysis of internal organs of treated mice. To test whether the tissue of internal organs was injured when IL-24-iRGD was administered *in vivo*, the heart, liver, spleen, lung, and kidney of mice were excised and analyzed by H&E staining (magnification, ×400). Data are expressed as the mean ± SD; ns, not significant. Scale bar = 50 μm.

the efficacy of IL-24 antitumor therapy, which may be used for the clinical treatment of patients with PCa in the future.

Disclosure of Potential Conflicts of Interest
No potential conflicts of interest were disclosed.

References

[1] Bray F, Ferlay J, Soerjomataram I, Siegel RL, Torre LA, and Jemal A (2018). Global cancer statistics 2018: GLOBOCAN estimates of incidence and mortality worldwide for 36 cancers in 185 countries. *CA Cancer J Clin* **68**, 394–424.

[2] Siegel RL, Miller KD, and Jemal A (2018). Cancer statistics, 2018. *CA Cancer J Clin* **68**, 7–30.

[3] Sarkar S, Quinn BA, Shen XN, Dash R, Das SK, Emdad L, Klibanov AL, Wang XY, Pellecchia M, and Sarkar D, et al (2015). Therapy of prostate cancer using a novel cancer terminator virus and a small molecule BH-3 mimetic. *Oncotarget* **6**, 10712–10727.

[4] Welch HG, Gorski DH, and Albertsen PC (2015). Trends in metastatic breast and prostate cancer—lessons in cancer dynamics. *N Engl J Med* **373**, 1685–1687.

[5] Jiang H, Lin JJ, Su ZZ, Goldstein NI, and Fisher PB (1995). Subtraction hybridization identifies a novel melanoma differentiation associated gene, mda-7, modulated during human melanoma differentiation, growth and progression. *Oncogene* **11**, 2477–2486.

[6] Fisher PB (2005). Is mda-7/IL-24 a "magic bullet" for cancer? *Cancer Res* **65**, 10128–10138.

[7] Menezes ME, Bhatia S, Bhoopathi P, Das SK, Emdad L, Dasgupta S, Dent P, Wang XY, Sarkar D, and Fisher PB (2014). MDA-7/IL-24: multifunctional cancer killing cytokine. *Adv Exp Med Biol* **818**, 127–153.

[8] Dent P, Yacoub A, Hamed HA, Park MA, Dash R, Bhutia SK, Sarkar D, Gupta P, Emdad L, and Lebedeva IV, et al (2010). MDA-7/IL-24 as a cancer therapeutic: from bench to bedside. *Anticancer Drugs* **21**, 725–731.

[9] Sauane M, Lebedeva IV, Su ZZ, Choo HT, Randolph A, Valerie K, Dent P, Gopalkrishnan RV, and Fisher PB (2004). Melanoma differentiation associated gene-7/interleukin-24 promotes tumor cell-specific apoptosis through both secretory and nonsecretory pathways. *Cancer Res* **64**, 2988–2993.

[10] Saito Y, Miyahara R, Gopalan B, Litvak A, Inoue S, Shanker M, Branch CD, Mhashilkar AM, Roth JA, and Chada S, et al (2005). Selective induction of cell cycle arrest and apoptosis in human prostate cancer cells through adenoviral transfer of the melanoma differentiation-associated–7 (mda-7)/interleukin-24 (IL-24) gene. *Cancer Gene Ther* **12**, 238–247.

[11] Sugahara KN, Teesalu T, Karmali PP, Kotamraju VR, Agemy L, Girard OM, Hanahan D, Mattrey RF, and Ruoslahti E (2009). Tissue-penetrating delivery of compounds and nanoparticles into tumors. *Cancer Cell* **16**, 510–520.

[12] Zhang Q, Zhang Y, Li K, Wang H, Li H, and Zheng J (2015). A novel strategy to improve the therapeutic efficacy of gemcitabine for non–small cell lung cancer by the tumor-penetrating peptide iRGD. *PLoS One* **10**e0129865.

[13] Teesalu T, Sugahara KN, Kotamraju VR, and Ruoslahti E (2009). C-end rule peptides mediate neuropilin-1–dependent cell, vascular, and tissue penetration. *Proc Natl Acad Sci U S A* **106**, 16157–16162.

[14] Yin H, Yang J, Zhang Q, Wang H, Xu J, and Zheng J (2017). iRGD as a tumor penetrating peptide for cancer therapy (Review). *Mol Med Rep* **15**, 2925–2930.

[15] Tian H, Wang J, Zhang B, Di J, Chen F, Li H, Li L, Pei D, and Zheng J (2012). MDA-7/IL-24 induces Bcl-2 denitrosylation and ubiquitin-degradation involved in cancer cell apoptosis. *PLoS One* **7**e37200.

[16] Zhang J, Sun A, Xu R, Tao X, Dong Y, Lv X, and Wei D (2016). Cell-penetrating and endoplasmic reticulum-locating TAT-IL-24-KDEL fusion protein induces tumor apoptosis. *J Cell Physiol* **231**, 84–93.

[17] Sugahara KN, Braun GB, de Mendoza TH, Kotamraju VR, French RP, Lowy AM, Teesalu T, and Ruoslahti E (2015). Tumor-Penetrating iRGD Peptide Inhibits Metastasis. *Mol Cancer Ther* **14**, 120–128.

[18] Shen Y, Yang F, Wang H, Cai Z, Xu Y, Zhao A, Su Y, Zhang G, and Zhu SX (2016). Arg-Gly-Asp (RGD)-modified E1A/E1B double mutant adenovirus enhances antitumor activity in prostate cancer cells in vitro and in mice. *PLoS One* **11**e0147173.

[19] Zheng DQ, Woodard AS, Fornaro M, Tallini G, and Languino LR (1999). Prostatic carcinoma cell migration via alpha(v)beta3 integrin is modulated by a focal adhesion kinase pathway. *Cancer Res* **59**, 1655–1664.

[20] Pallaoro A, Braun GB, and Moskovits M (2011). Quantitative ratiometric discrimination between noncancerous and cancerous prostate cells based on neuropilin-1 overexpression. *Proc Natl Acad Sci U S A* **108**, 16559–16564.